https://doi.org/10.5194/essd-2019-194
Preprint. Discussion started: 30 October 2019

Open Access Earth System Science Data Discussions

High-resolution (1 km) Polar WRF output for 79°N Glacier and the Northeast of Greenland from 2014-2018

Jenny. V. Turton[1], Thomas Mölg[1], Emily Collier[1]

[1]Climate System Research Group, Institute of Geography, Friedrich-Alexander University, Erlangen-Nürnberg, 90158, Germany

Correspondence to: Jenny V. Turton (jenny.turton@fau.de)

Abstract.

The northeast region of Greenland is of growing interest due to changes taking place on the large marine-terminating glaciers which drain the north east Greenland ice stream. Nioghalvfjerdsfjordern, or 79°N glacier, is one of these glaciers that is currently experiencing accelerated thinning, retreat and enhanced surface melt. Understanding both the influence of atmospheric processes on the glacier and the interactions between the atmosphere and the changing surface is crucial for our understanding of present stability and future change. However, relatively few studies have focused on the atmospheric processes in this region, and even fewer have used high-resolution modelling as a tool for these research questions. Here we present a high-resolution (1 km) atmospheric modelling dataset, NEGIS_WRF, for the 79°N and northeast Greenland region from 2014-2018, and an evaluation of the model's success at representing daily near-surface meteorology compared with two automatic weather station records. The dataset, (Turton et al, 2019b: doi.org/10.17605/OSF.IO/53E6Z), is now available for a wide variety of applications ranging from atmospheric dynamics, to input for hydrological and oceanic modelling studies.

1 Introduction

The large amount of mass lost from the Greenland Ice Sheet (GrIS) within the last decade has largely been located around the coast of Greenland, due to the thinning and retreat of marine-terminating glaciers (Schaffer et al., 2017), and the surface mass loss in the ablation zone (Rignot, et al, 2015; van den Broeke et al., 2017). The surface mass balance of a glacier is largely controlled by regional climate through varying mass gains and losses in the ablation and accumulation zones, respectively. The majority of studies of the surface mass loss in Greenland and its atmospheric controls are largely constrained to southern and western Greenland (e.g Kuipers Munneke et al., 2018; Mernild et al., 2018), or to specific warm events such as the 2012 melt event (e.g Bennartz et al., 2013; Tedesco et al., 2013). However, recent studies have shown that the northeast of Greenland, specifically the North East Greenland Ice Steam (NEGIS) is now experiencing high ice velocity and accelerated thinning rates (Joughin et al., 2010; Khan et al., 2014). NEGIS extends into the interior of the Greenland ice stream by 600 km and three marine-terminating glaciers connect the NEGIS with the ocean. The largest of these glaciers is Nioghalvfjerdsfjorden,

https://doi.org/10.5194/essd-2019-194
Preprint. Discussion started: 30 October 2019

often named 79°N after its latitudinal position. Until recently, very few studies focused on 79°N glacier and NEGIS as they were thought to contribute little to surface mass loss and instabilities (Khan et al., 2014; Mayer et al., 2018). However, 79°N glacier, with its 80 km long by 20 km wide floating tongue, has retreated by 2-3km between 2009 and 2012, and is now thinning at a rate of 1 m yr^{-1}(Khan et al., 2014). This glacier is now of interest due to its potential change in stability, and because its southerly neighbour, Zachariae Istrom, recently lost its floating tongue (Mouginot et al., 2015).

A number of studies have used modelling as a tool to investigate the region, although they have largely been confined to short case studies (Turton et al., 2019), focused on oceanic processes (Mayer et al., 2018; Schaffer et al., 2017), focused on past climates (e.g 45000 years ago by Larsen et al., 2018) or targeted specific atmospheric processes (Leeson, et al., 2018; Turton et al., 2019a). There are a number of atmospheric models that have been applied to the Greenland region, however these are often run at a resolution that is too coarse to resolve the 79°N glacier, especially its floating tongue, which can therefore be missing in many simulations. These data are usually statistically downscaled to calculate the surface mass balance of the glacier, using a digital elevation model and a shape file of the glacier. The resolution of the atmospheric models used in published studies for Greenland generally exceed 10km: e.g the Modèle Atmosphérique Régional (MAR) at 20-km (Fettweis et al., 2017), RACMO2 at 11-km (Noël et al., 2016) and HIRHAM5 at 25-km (Mottram et al., 2017).

As yet, there are no very high-resolution multi-year atmospheric datasets for this region. Here, we address this data gap by presenting a novel 5-year (2014-2018), high resolution (1 km) atmospheric simulation using a polar-optimised atmospheric model and evaluate its skill in representing local meteorological conditions over the 79°N region in northeast Greenland. The dataset is named NEGIS_WRF after its location of focus and model used. As the 79°N region is of growing interest, this data could be beneficial for numerous other studies and applications. Indeed, current ongoing research as part of the Greenland Ice sheet-ocean interaction (GROCE) project (www.groce.de, last accessed October 1 2019) include using this data for surface mass balance studies and to investigate the relationship between specific atmospheric processes and surface melt patterns. For studies of the surface mass balance of the NEGIS, further downscaling would not be necessary. Furthermore, at this resolution, many atmospheric processes are accurately resolved including katabatic winds and warm-air advection (Turton et al., 2019a). The WRF dataset is also intended as input to an ocean model, used in an ocean-glacier interaction study, input into a hydrologic model and for an ice sheet modelling study. To demonstrate the applicability/suitability of the dataset for these and other studies in the fields of atmospheric, cryospheric and oceanic fields, in this manuscript we present an evaluation of the ability of NEGIS_WRF at representing key near-surface meteorological conditions, to inform future users of its skill.

https://doi.org/10.5194/essd-2019-194
Preprint. Discussion started: 30 October 2019

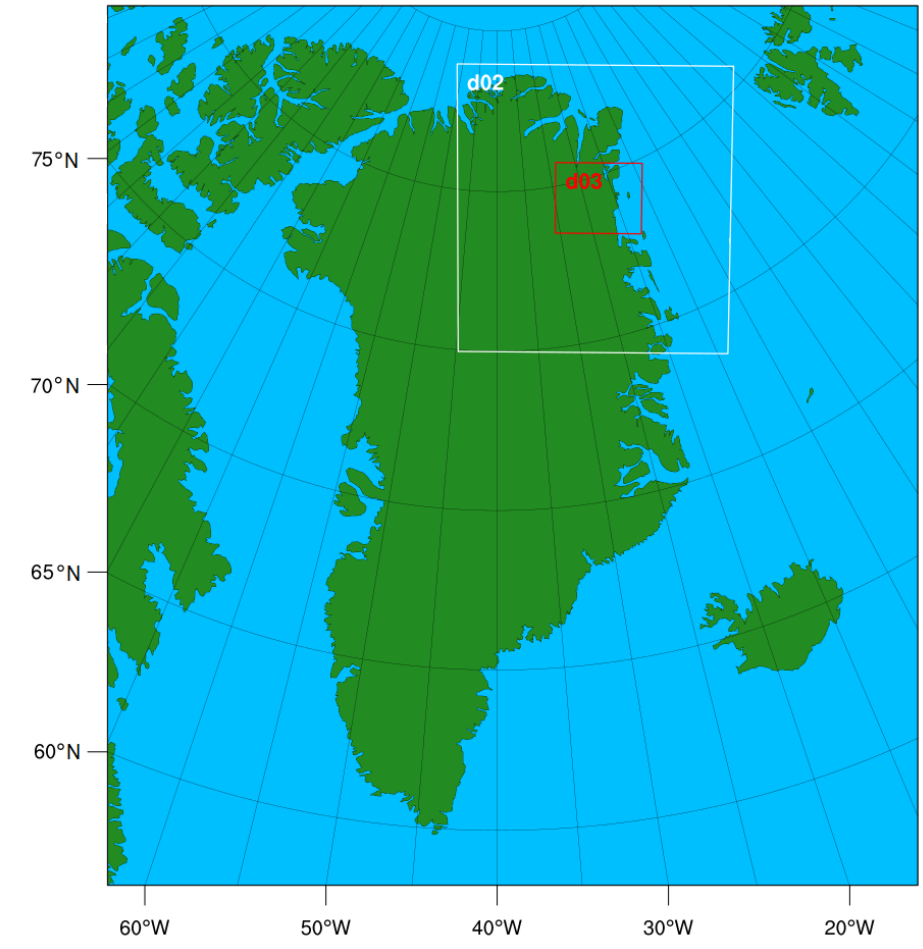

Figure 1: The three domain setup for the Polar WRF runs.

2. Data and Methods

2.1 Model Configuration

The Polar Weather Research and Forecasting (Polar WRF) model is a version of the WRF model that was developed and optimised for use in polar climates (Hines et al., 2011). The non-hydrostatic WRF model (available online from http://www.mmm.ucar.edu/weather-research-and-forecasting-model; last accessed July 29 2019) has been widely used for both operational studies and for research in many regions, and at many scales (Powers et al., 2017; Skamarock & Klemp, 2008). The current version of polar WRF used here is v3.9.1.1, which was released in January 2018, and is available from

https://doi.org/10.5194/essd-2019-194
Preprint. Discussion started: 30 October 2019

http://polarmet.osu.edu/PWRF/ (last accessed July 29 2019). Polar WRF has been developed for use in the Arctic and Antarctic by largely optimising the Noah Land Surface Model (LSM) to improve heat transfer processes through snow and permanent ice, and by providing additional methods for sea-ice treatment (Hines et al, 2015). For a full description of the Polar WRF additions, please see (Hines & Bromwich, 2008; Hines et al., 2011; Hines et al, 2015) and citations therein.

The meteorological initialisation and boundary input data is from the ECMWF (European Centre for Medium range Weather Forecast) ERA-Interim dataset at 6-hourly intervals (Dee et al., 2011). This reanalysis product was more accurate at resolving mesoscale processes in the northeast of Greenland compared to other sources and has previously been used to initialise WRF in this region (Turton et al., 2019a). The Sea Surface Temperature (SST) and sea ice concentration data are from the 0.25° resolution daily, Advanced Very High Resolution Radiometer (AVHRR) infrared satellite data (doi:10.5065/EMOT-1D34, data retrieved from https://rda.ucar.edu/datasets/ds277.7/, last accessed July 29 2019). This higher resolution dataset was required due to the very blocky coastline in the SST and sea ice data from ERA-Interim. These data have previously been used for Greenland in Polar WRF (DuVivier, & Cassano, 2013; Turton et al., 2019a). Boundary conditions, including sea ice fraction and SST are updated every 6-hours. Analysis nudging was used in the outer domain (D01) to constrain the large-scale circulation while allowing the model to freely simulate in D02 and D03. The domain set up is shown in Figure 1. The USGS 24 category landuse and landmask was adjusted using the European Space Agency (ESA) Climate Change Initiative (CCI) landuse product, to provide a better representation of the glacier outlines and the terminus of the floating tongue (https://www.esa-landcover-cci.org/, last accessed September 5 2019). A number of open-water grid points were manually changed to glacierised during January-June and September-December to better represent the floating tongue of the Spalte Glacier (tributary of 79°N on the northeast side) and the sea ice in the adjacent Dijmphna Sound (Fig. 2) and other small exposed water areas along the coast, which are permanently frozen, except in July and August each year (Hochreuther, P., 2019 personal communication). The glacier extents are treated as static throughout the run, which is an appropriate approximation given the small area of calving at 79°N during this period. The outermost domain (D01) is at 25km, D02 is 5km and D03 (innermost) is 1km grid spacing. There are 60 levels in the vertical, with a 10-hPa model top and a lowest model level ~16m above the surface.

Many of the parameterisations for the model configuration were selected based on numerous, previous Polar WRF runs over Greenland and the Arctic (for example Hines et al., 2011). In brief, the following parameterisations were employed: the Noah LSM, due to its optimisations that have been tested over Greenland (Hines & Bromwich, 2008),Arctic sea ice (Hines, et al 2015) and Arctic land (Hines et al., 2011); the Morrison two-moment scheme for microphysics, which has been shown to out-perform other schemes in both Polar regions (Bromwich, et al., 2009; Lachlan-Cope, et al., 2016; Listowski & Lachlan-Cope, 2017); the Eta Similarity Scheme for surface layer physics (Janjić, 1994) and the Yonsei University Scheme for planetary boundary layer parameterisation, due to the topographic wind scheme (Hong et al., 2006) that can correct excessive wind speeds in areas of complex topography, such as the northeast coast of Greenland (employed in D02 and D03 only, where complex orography is best resolved); the Kain-Fritsch scheme for cumulus convection (Kain, 2004) (D01 and D02 only); and, the Rapid Radiative Transfer Model (RRTM) longwave and Goddard shortwave schemes for radiation, based on sensitivity

https://doi.org/10.5194/essd-2019-194
Preprint. Discussion started: 30 October 2019

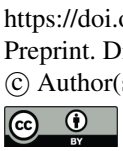

testing for the polar regions by Hines et al. (2008) and subsequent runs over Greenland (DuVivier & Cassano, 2013; Hines et al., 2011). Whilst the majority of these options were selected for testing based on the works of other publications, a short sensitivity study was also conducted, alongside with testing the horizontal and vertical resolution and locations of the domains (not included). It was found that a combination of the options above were best suited to the northeast of Greenland when compared with observations on the floating tongue of the 79°N glacier from 1996-1999 (Turton et al., 2019a).

Other options specified for this study include using a fractional sea ice treatment, which allows calculation of different surface temperature, surface roughness and turbulent fluxes for open water and sea ice conditions within the grid cell, and then calculates an area-weighted average for the grid (DuVivier & Cassano, 2013; Hines et al., 2011). The adaptive timestep was used to optimise the simulation speed. For each year simulated, the model was initialised on September 1 and ran continuously until October 1 of the following year (e.g September 1 2016 - October 1 2017). September was then discarded as a spin up month. The model was initialised in September so that the snowpack was adequately spun up before the onset of the accumulation season. The data were output at hourly intervals for D3, at six-hourly intervals for D2 and at daily intervals for D1. Daily mean values for key meteorological variables from D2 and D3 were calculated from the hourly values and are available along with the daily instantaneous values from D1 at the Open Science Framework repository (Turton et al 2019b: doi.org/10.17605/OSF.IO/53E6Z).

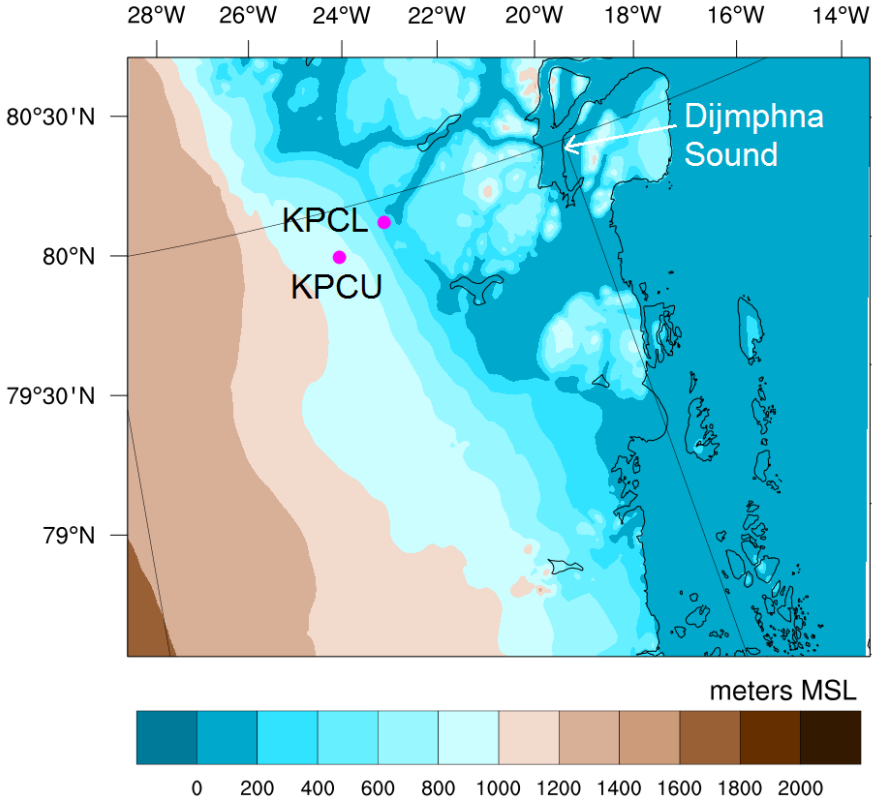

https://doi.org/10.5194/essd-2019-194
Preprint. Discussion started: 30 October 2019

Figure 2: The topography and coastline of D03, with the location of the two AWSs and Dijmphna Sound.

2.2 Observational Data

The remote nature of the location of interest provides few in-situ observational datasets for model evaluation. However, the PROMICE (Programme for Monitoring of the Greenland Ice Sheet) network (www.promice.dk, last accessed October 1 2019; van As & Fausto, 2011), operated by the Geological Survey of Denmark and Greenland (GEUS) has two permanent Automatic Weather Stations (AWSs) available for comparison of daily means of meteorological variables and a number of surface energy balance components. The AWSs are referred to as KPC_L and KPC_U due to their location on Kronprincs Christian Land (located to the northwest of 79°N glacier (see Table 1 for AWS details of location, dates and available variables). Although hourly data are available, daily means are used for evaluation due to the multi-year timescale of the study, but the authors note that an evaluation of hourly data should be performed before using these data for analysis at these time scales. Please refer to van As & Fausto, (2011) and Turton et al., (2019a) for more information on the PROMICE data in this location (doi.org/10.22008/promice/data/aws, available at www.promice.dk, last accessed October 1 2019).

Table 1: The location, elevation and data availability of the two AWSs used for model evaluation. We evaluate the model output with four variables from the AWSs, please see van As & Fausto, (2011) for more information. Data was unavailable at KPC_L between January 15 2010 and July 17 2012 due to retrieval problems. T2 is air temperature at 2m, Q2 is specific humidity at 2m, WS10 and WD10 are wind speed and direction at 10m, respectively.

AWS name	**Location**	**Elevation (m a.s.l)**	**Data Availability**	**Variables used for evaluation**
KPC_L	79.91, -24.08	370	01.01.2009- present	T2, Q2, WS10, WD10
KPC_U	79.83, -25.17	870	01.01.2009-14.01.2010, 18.07.2012-present	T2, Q2, WS10, WD10

2.3 Model Evaluation

Output from NEGIS_WRF have been evaluated against in-situ AWS observations from two locations to the northwest of the 79°N glacier (Fig 2). The focus of the evaluation is to test WRF's ability to represent local meteorological conditions over a polar glacier, to provide insight to the skill of the dataset for future use. The first set of evaluation focuses on daily mean values and is followed by an evaluation of how WRF represents daily maxima and minima, as well as the mean diurnal cycle of air

https://doi.org/10.5194/essd-2019-194
Preprint. Discussion started: 30 October 2019

temperature. Only air temperature is assessed on a sub-daily scale due to its importance in many applications. All evaluation focuses on near-surface meteorological output from D3. Daily mean values have been calculated from hourly output data at the location of the two AWSs. The mean values from the observational data are calculated from daily averages from January 1 2014- December 31 2018 to keep a consistent period across all data.

3. Results

3.1 Daily mean evaluation

Table 2: Comparison of the near-surface WRF model output to AWS data at KPC_L and KPC_U. ANN refers to annual mean values, DJF refers to winter average values whereas JJA refers to summer average values. Mean bias represents the model-observations. * refers to statistically significant differences between the model and observations at the 95% confidence interval (is 99% confidence interval), using the student's t-test.**

Variable (units)	Location	AWS Mean	Mean Bias	RMSE	Correlation
T2 ANN (°C)	KPCL	-13.6	-0.3	3.0	0.96
	KPCU	-17.2	1.8	4.0	0.96
T2 DJF (°C)	KPCL	-23.3	0.0	3.2	0.93
	KPCU	-27.6	2.6	5.2	0.8
T2 JJA (°C)	KPCL	1.6	-1.8	2.6	0.84
	KPCU	-1.5	-0.1	1.9	0.83
Q2 ANN (g/kg)	KPCL	1.6	0.2	0.4	0.96
	KPCU	1.4	0.3	0.5	0.96
Q2 DJF (g/kg)	KPCL	0.4	0.1	0.1	0.90
	KPCU	0.3	0.1	0.2	0.81
Q2 JJA (g/kg)	KPCL	3.2	0.4	0.8	0.66
	KPCU	3.0	0.6**	0.9	0.75
WD ANN (°)	KPCL	219.4	10.7**	74.3	0.1
	KPCU	277.9	3.4	29.9	0.6
WD DJF (°)	KPCL	238.5	-3.2	49.9	0.1
	KPCU	274	8.6	29.1	0.6
WD JJA (°)	KPCL	211.6	6.8**	80.2	0.1
	KPCU	279.9	-0.1	31.7	0.5
WS ANN (m/s)	KPCL	5.7	0.4	2.9	0.65
	KPCU	4.8	1.5	2.5	0.7

https://doi.org/10.5194/essd-2019-194
Preprint. Discussion started: 30 October 2019

Open Access Earth System Science Data Discussions

WS DJF (m/s)	**KPCL**	**6.4**	**1.0**	**3.2**	**0.71**
	KPCU	**5.2**	**2.3**	**3.4**	**0.62**
WS JJA (m/s)	**KPCL**	**5.4**	**-0.8**	**2.7**	**0.56**
	KPCU	**4.2**	**0.8**	**1.9**	**0.67**

The air temperature is simulated well by the WRF simulations with an annual correlation of 0.96 at both KPCL and KPCU (Table 2, Fig 3). Similarly, the mean biases and RMSE are small. The mean bias and RMSE are slightly larger during winter (DJF) at KPCU, but overall, the correlation at both locations remains above 0.8. The particularly low daily temperatures observed during winter at KPCU are not fully captured by the WRF simulations (Fig. 3b). The model can, however, capture the larger variability in winter (Fig. 3), including 'warm-air events', where the air temperature increases by more than 10°C in a short period of time, leading to temperatures above the average for winter (Turton et al., 2019a). WRF also simulates the humidity very well annually and during winter for both locations, with annual correlations of 0.96. The humidity during summer is slightly less well simulated, with mean biases of 0.4 and 0.6 g/kg for KPCL and KPCU respectively (Table 2). However, the correlations remain above 0.65 for the summer season. For both locations, annually and seasonally, WRF is moister than in observations, however the mean biases remain relatively small (less than 0.6 g/kg), and the differences are not statistically significant except for during summer at KPCU (which is statistically different at the 99% confidence level using a student t-test). The representation of the wind direction in WRF is more variable than for temperature and moisture. The largest bias is an annual bias at KPCL (10.7°) as WRF simulates the wind direction predominantly more northerly than in observations (Table 2), which leads to poor correlations (0.1) and high RMSE. For KPCU annually and seasonally, the biases remain at or below 8.6° and correlation coefficients are 0.6, which shows that WRF is capable of representing the wind direction well at KPCU. The wind speed is simulated better than the wind direction. Annually and during winter, the correlations are relatively high (above 0.56) at both locations, and mean biases remain at or below 2.3 ms^{-1} both annually and seasonally. None of the biases between WRF and observations are statistically significantly different for daily mean wind speed or air temperature (Table 2).

The larger RMSE and lower correlation during summer for wind direction can, at least partly, be attributed to the larger variability of those variables during summer. In summer (JJA), the average deviation of wind direction in observations at KPCL is 40.3°. Whilst WRF is able to capture this variability in wind direction (the average deviation is 41.1°), there is sometimes an offset in the timing of the wind direction change between WRF and observations. For example, after two weeks of consistently northwesterly winds being observed at KPCL between August 11 to 24 2014, there was a shift to northeasterly flow on the morning of August 25 2014 (Fig 4e). WRF successfully simulated the long period of northwesterly winds, and the shift to winds from the northeast, however the change in direction was simulated in the late evening of August 25 to early morning of August 26 (Fig. 4f), leading to a bias of 156.9° on August 25. The northeasterly wind was only observed for 24-hours before returning to westerly on August 26 (Fig. 4g). WRF was able to capture the short-lived timing of the event, but

https://doi.org/10.5194/essd-2019-194
Preprint. Discussion started: 30 October 2019


Open Access Earth System Science Data Discussions

24-hours later. In this particular case, the wind direction error comes from the boundary data, ERA-Interim. In ERA-Interim, the wind direction change starts on August 24 but remains northerly until 18:00UTC on August 25. It then remains northeasterly until August 27, which is 24-hours longer than in near-surface observations. The later onset and more persistent flow from the northeast in ERA-Interim likely led to the later onset of northeasterly flow in WRF. Therefore, WRF can capture both the predominant wind flow, and abrupt changes to the wind direction, along with capturing even short-lived events, although the timing is occasionally shifted. Figure 4 also highlights that whilst the mean bias for wind speed is less than 1.5 ms^{-1} (Table 2), during individual cases, WRF can simulate much higher wind speeds than observed.

Overall, WRF performs well at simulating air temperature, humidity and wind speed during the simulation period (Oct 2013 - Dec 2018). WRF struggles to as accurately represent the wind direction, especially at KPCL, however the winds remain predominantly westerly to northwesterly, which shows that WRF can capture the dominant katabatic process governing the wind directions.

https://doi.org/10.5194/essd-2019-194
Preprint. Discussion started: 30 October 2019

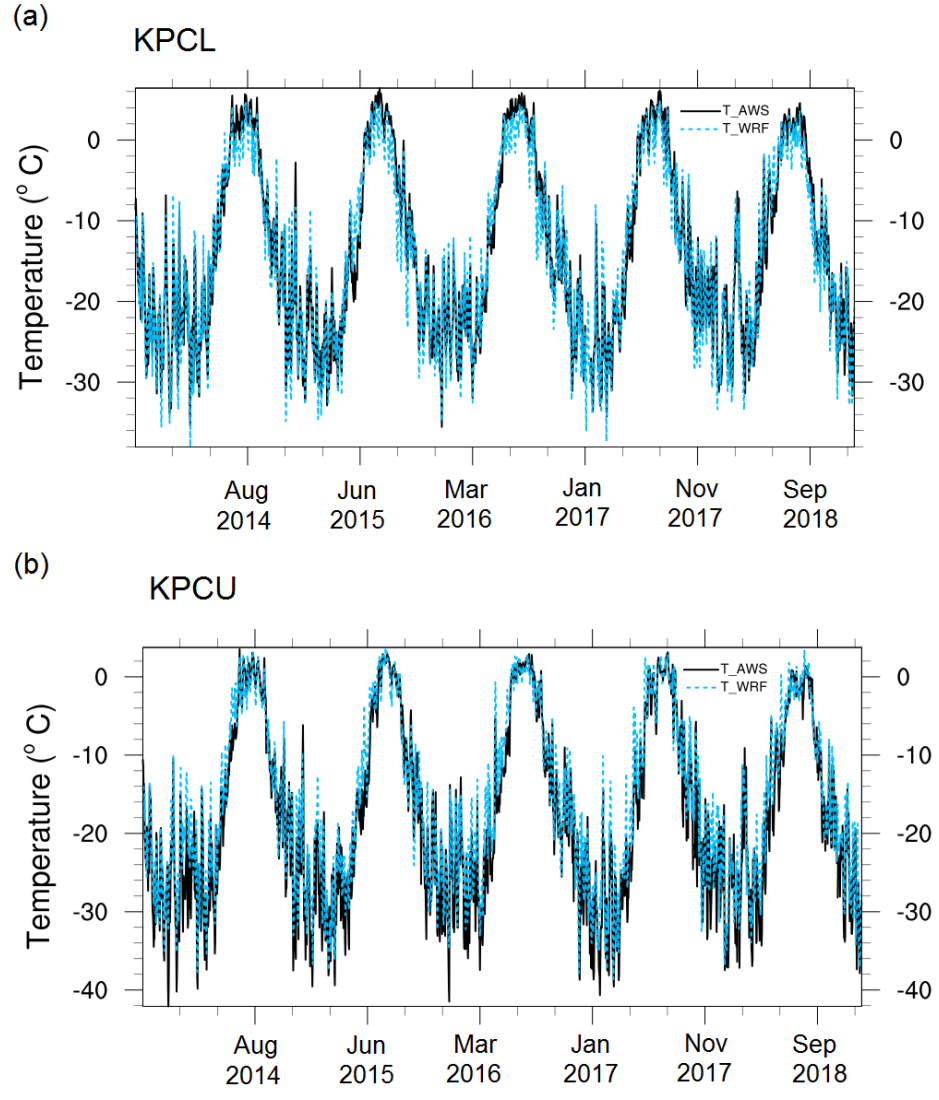

Figure 3: The observed (black lines) and modelled (dashed blue lines) daily averaged air temperature at KPCL (top) and KPCU (bottom).

https://doi.org/10.5194/essd-2019-194
Preprint. Discussion started: 30 October 2019

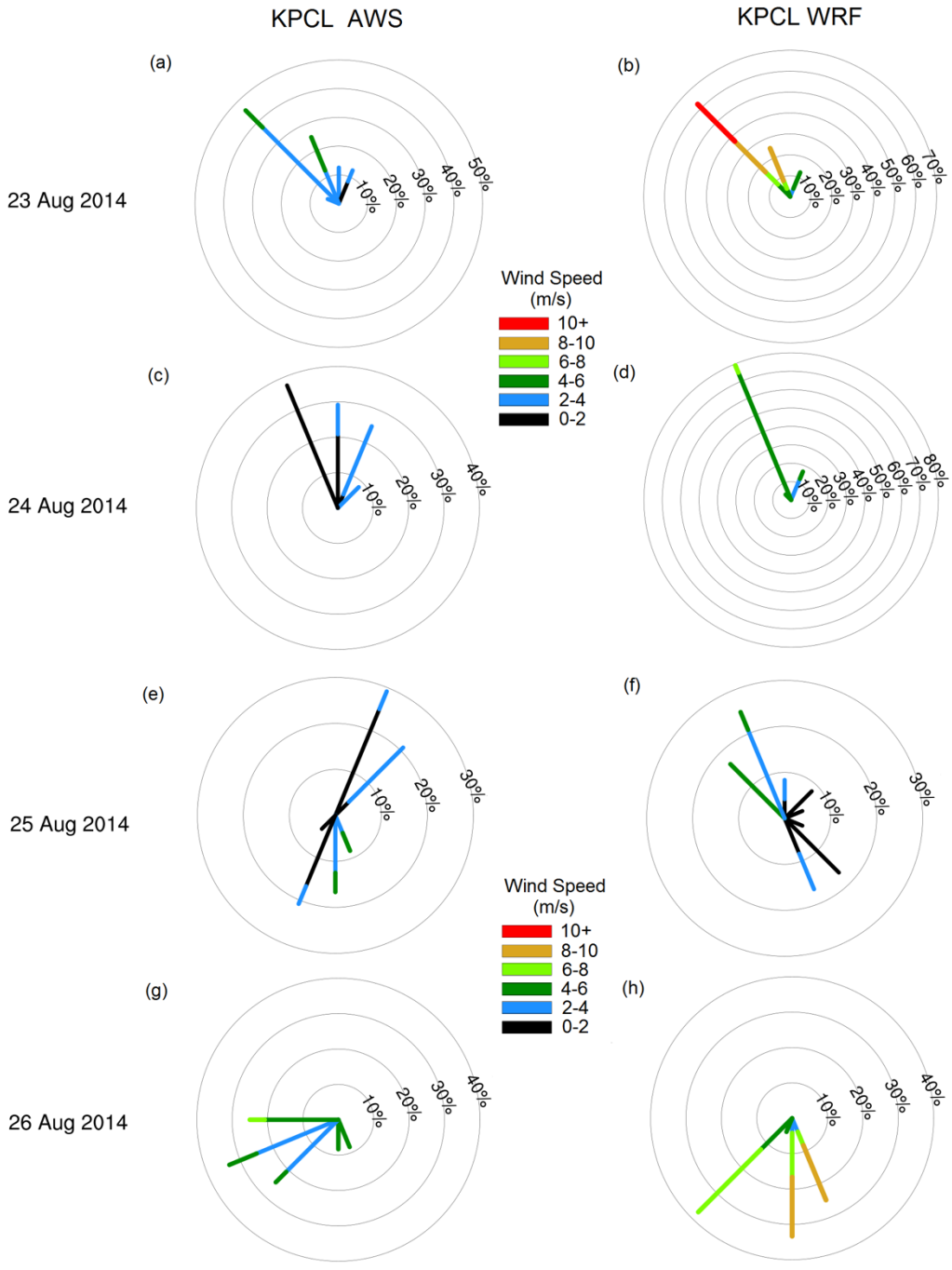

Figure 4: Wind speed (colour) and direction (lines) for August 23 to 26 2014 from observations (left panel) and WRF (right panel) at KPCL location.

https://doi.org/10.5194/essd-2019-194
Preprint. Discussion started: 30 October 2019

3.2 Sub-daily evaluation

To evaluate the ability of the model to simulate sub-daily values, the minimum and maximum daily near-surface values (from hourly output) are compared to observations, and the amplitude of the diurnal cycle of air temperature is also evaluated. Figure 5 presents the statistics for daily minimum and maximum air temperatures at the two locations in observations and WRF. The median values are well captured by WRF, especially for the maximum daily values, where a median value of -13.9°C is observed at KPCU, and -14.0°C is simulated. Similarly, for maximum temperatures, the 75th quartile values are well captured by WRF (Fig. 5). For KPCL, the minimum and maximum temperatures are colder in WRF than in observations. For example, the 25th percentile value for the minimum temperatures (far left bar in Fig. 5) is 3.8°C in observations, but 6.3°C in WRF. At KPCU, the opposite is true, where WRF simulates slightly higher temperatures than in observations. However, overall, the range of minimum and maximum temperature values are well modelled by WRF.

The average daily maximum air temperature observed at KPCL is -21.0°C in winter (DJF) and increases to 3.0°C in summer (JJA). WRF simulates an average daily maximum of -20.9°C in winter, which increases to 0.9°C in summer. The average daily minimum air temperature observed at KPCL is –25.9°C during winter and rises to 0.2°C in summer. WRF simulates an average daily minimum air temperature of -26.5°C in winter and increasing to -2.3°C in summer. Therefore, WRF is able to accurately simulate the winter minimum and maximum temperatures, but underestimates the air temperature during summer.

Similarly, at KPCU, the observed maximum temperature values are -24.1°C in winter and 0.1°C in summer. From WRF, the average maximum temperature is -22.5°C in winter and increases to -0.1°C in summer. The observed minimum daily air temperature at KPCU is -30.8°C during winter and –3.5°C in summer. In comparison, in the WRF simulations, the average daily minimum temperature is -27.4°C during winter and increases to -3.9°C in summer. WRF can therefore represent the maximum and minimum daily air temperatures at KPCU.

The annual-average observed diurnal air temperature amplitude is 5.6°C at KPCU and 4.0°C at KPCL. The largest average diurnal cycle is observed during spring (MAM) at KPCU (6.8°C) and during winter at KPCL (4.9°C). The WRF model simulated an average diurnal amplitude of 5.0°C at KPCU 4.7°C at KPCL. The largest diurnal cycles are simulated during spring at KPCU (6.2°C) and during winter at KPCL (5.5°C). Therefore, WRF accurately simulates the timing of the largest diurnal amplitudes but overestimates the amplitude slightly at KPCL, and underestimates it at KPCU, both by 0.6°C. The relatively large diurnal amplitude in winter may be counterintuitive given that the glacier is located in the Arctic, where polar night (no solar radiation) prevails throughout winter. However, the temperature variability is largest during winter over the glacier due to the occurrence of ‘warm-air events’ due to warm-air advection from the Atlantic and turbulent mixing from katabatic winds (Turton et al., 2019a).

The absolute maximum hourly air temperature over the four years of data observed at KPCL was on July 23 2014 (8.1°C) (Fig. 5). WRF was able to replicate the processes responsible for the particularly warm day, as a daily maximum value of 4.5°C was modelled at KPCU. At KPCL, the maximum was simulated 24-hours earlier (6.5°C). The maximum values from

https://doi.org/10.5194/essd-2019-194
Preprint. Discussion started: 30 October 2019

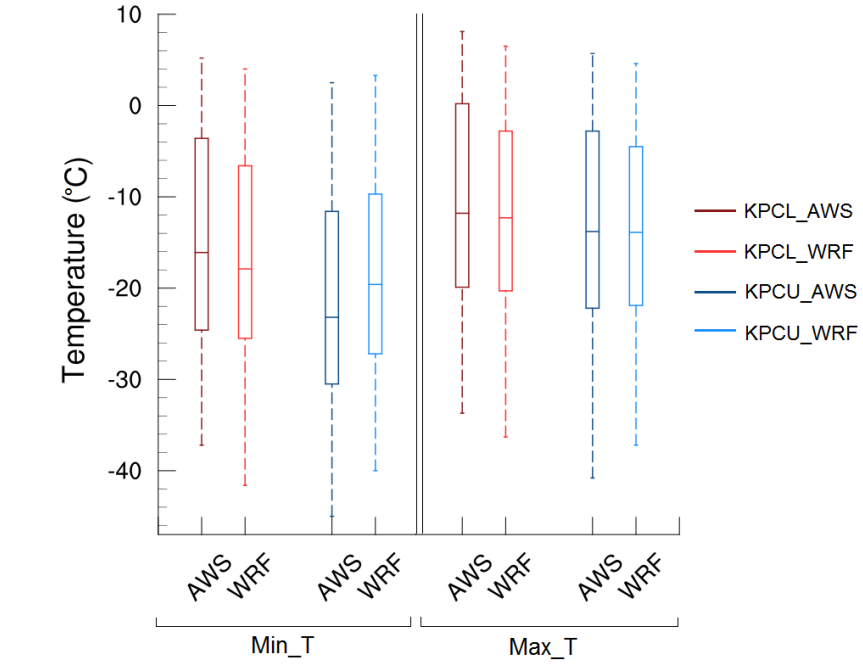

Figure 5: Box plot representing the minimum (left) and maximum (right) daily temperature values at KPCL (red) and KPCU (blue) locations, from both observations (darker colours) and WRF (lighter colours).

5. Conclusions

Polar WRF has previously been extensively used in the Arctic (e.g Hines et al., 2011; Hines, & Bromwich, 2017; Wilson, et al., 2011), including for Greenland (e.g DuVivier & Cassano., 2013; Turton et al., 2019a), for a number of applications. However, WRF runs have often been used for short case studies, or performed at lower spatial resolution. This dataset provides high spatial and temporal resolution runs over multiple years (2014-2018) for an area of increased interest. Regardless of the regular use of Polar WRF, it remains important to validate the model for specific locations, especially when downscaling to very high resolutions.

Overall, the mean biases are small and statistically insignificant between the Polar WRF runs and the PROMICE observations at both the lower and upper stations near 79°N glacier. The correlations are high for air temperature, humidity

https://doi.org/10.5194/essd-2019-194
Preprint. Discussion started: 30 October 2019

and wind speed, but less so for wind direction at KPCL. The wind direction is more variable in summer than in other months, and whilst WRF is able to simulate the increased variability, large biases can arise due to inconsistent timing of wind direction changes between WRF and observations over short periods of 24-hours or less. However, as WRF is able to replicate the short-lived events and the predominant northwesterly winds of katabatic origin, we can conclude that the NEGIS_WRF can be used for further studies of the near-surface meteorology of the 79°N glacier. This dataset will be useful for many other applications in a number of fields including the atmospheric and cryospheric, and as input to hydrological, ice sheet and ocean models.

4. Data Availability

The atmospheric dataset, NEGIS_WRF resolves for the first time, the meteorological conditions over the northeast region of Greenland (5km) and 79°N glacier region at the kilometre scale over a period of five years (2014-2018). More 50 variables are available (near-surface and on 60 atmospheric levels) at up to hourly temporal resolution (for the 1 km domain), including meteorological and radiative fields. Daily mean values for near-surface temperature (2m), specific humidity (2m), skin temperature, and U and V wind components (10m) are available online (Turton et al 2019b: doi.org/10.17605/OSF.IO/53E6Z) for the 1km and 5km domains from 2014-2018. As the output frequency from D01 (25km resolution) was once per day, the available values are instantaneous daily values at 00 UTC, as opposed to daily means. Furthermore, 4-D variables of temperature, humidity, U and V wind components, geopotential and pressure are available on model levels at the same frequency as the near-surface variables. For other variables, or more frequent output, please contact the lead author, and these can be made available. Due to the large amount of data, these are not stored online, but at the Regional Computation Centre Erlangen (RRZE) in Germany.

6. Author Contributions

JVT wrote the paper, ran the WRF model and evaluated it against the observations. TM and EC contributed to the discussion optimisation of the simulations and manuscript refinement.

7. Competing Interests

The authors have no competing interests

8. Acknowledgements

We thank Dirk van As from GEUS for his assistance with the PROMICE data and to Keith Hines for the Polar WRF code. This work was supported by the German Federal Ministry for Education and Research (BMBF) and forms part of the GROCE project (Greenland Ice Sheet/Ocean Interaction) (Grant 03F0778F). We acknowledge the High Performance Computing Centre (HPC) at the University of Erlangen-Nürnberg's Regional Computation Centre (RRZE), for their support and resources whilst running the Polar WRF simulations.

9. References

Bennartz, R., Shupe, M. D., Turner, D. D., Walden, V. P., Steffen, K., Cox, C. J., … Pettersen, C. (2013). July 2012 Greenland

https://doi.org/10.5194/essd-2019-194
Preprint. Discussion started: 30 October 2019

melt extent enhanced by low-level liquid clouds. *Nature*, *496*(7443), 83–86. https://doi.org/10.1038/nature12002

Bromwich, D. H., Hines, K. M., & Bai, L. (2009). Development and testing of Polar Weather Research and Forecasting model: 2. Arctic Ocean. *Journal of Geophysical Research*, *114*(D8), D08122. https://doi.org/10.1029/2008JD010300

Dee, D. P., Uppala, S. M., Simmons, A. J., Berrisford, P., Poli, P., Kobayashi, S., … Vitart, F. (2011). The ERA-Interim reanalysis: configuration and performance of the data assimilation system. *Quarterly Journal of the Royal Meteorological Society*, *137*(656), 553–597. https://doi.org/10.1002/qj.828

DuVivier, A. K., & Cassano, J. J. (2013). Evaluation of WRF Model Resolution on Simulated Mesoscale Winds and Surface Fluxes near Greenland. *Monthly Weather Review*, *141*(3), 941–963. https://doi.org/10.1175/MWR-D-12-00091.1

European Space Agency Climate Change Initiative landuse product, available from https://www.esa-landcover-cci.org/, last accessed September 5 2019.

Fausto, R.S and van As, D. (2019). Programme for monitoring of the Greenland ice sheet (PROMICE): Automatic weather station data. Version: v03, Dataset published via Geological Survey of Denmark and Greenland. https://doi.org/10.22008/promice/data/aws

Fettweis, X., Box, J. E., Agosta, C., Amory, C., Kittel, C., Lang, C., … Gallée, H. (2017). Reconstructions of the 1900–2015 Greenland ice sheet surface mass balance using the regional climate MAR model. *The Cryosphere*, *11*(2), 1015–1033. https://doi.org/10.5194/tc-11-1015-2017

Hines, K. M., & Bromwich, D. H. (2008). Development and Testing of Polar Weather Research and Forecasting (WRF) Model. Part I: Greenland Ice Sheet Meteorology*. *Monthly Weather Review*, *136*(6), 1971–1989. https://doi.org/10.1175/2007MWR2112.1

Hines, K. M., Bromwich, D. H., Bai, L.-S., Barlage, M., Slater, A. G., Hines, K. M., … Slater, A. G. (2011). Development and Testing of Polar WRF. Part III: Arctic Land*. *Journal of Climate*, *24*(1), 26–48. https://doi.org/10.1175/2010JCLI3460.1

Hines, K. M., Bromwich, D. H., Bai, L., Bitz, C. M., Powers, J. G., Manning, K. W., … Manning, K. W. (2015). Sea Ice Enhancements to Polar WRF*. *Monthly Weather Review*, *143*(6), 2363–2385. https://doi.org/10.1175/MWR-D-14-00344.1

Hines, K. M., & Bromwich, D. H. (2017). Simulation of Late Summer Arctic Clouds during ASCOS with Polar WRF. *Monthly Weather Review*, *145*(2), 521–541. https://doi.org/10.1175/MWR-D-16-0079.1

Hochreuther, P, Friedrich Alexander Universtiy, Personal Communication, July 2019

Hong, S.-Y., Noh, Y., Dudhia, J., Hong, S.-Y., Noh, Y., & Dudhia, J. (2006). A New Vertical Diffusion Package with an Explicit Treatment of Entrainment Processes. *Monthly Weather Review*, *134*(9), 2318–2341. https://doi.org/10.1175/MWR3199.1

Janjić, Z. I. (1994). The Step-Mountain Eta Coordinate Model: Further Developments of the Convection, Viscous Sublayer, and Turbulence Closure Schemes. *Monthly Weather Review*, *122*(5), 927–945. https://doi.org/10.1175/1520-0493(1994)122<0927:TSMECM>2.0.CO;2

Joughin, I., Smith, B. E., Howat, I. M., Scambos, T., & Moon, T. (2010). Greenland flow variability from ice-sheet-wide

https://doi.org/10.5194/essd-2019-194
Preprint. Discussion started: 30 October 2019

velocity mapping. *Journal of Glaciology*, *56*(197), 415–430. https://doi.org/10.3189/002214310792447734

Kain, J. S. (2004). The Kain–Fritsch Convective Parameterization: An Update. *Journal of Applied Meteorology*, *43*(1), 170–181. https://doi.org/10.1175/1520-0450(2004)043<0170:TKCPAU>2.0.CO;2

Khan, S. A., Kjær, K. H., Bevis, M., Bamber, J. L., Wahr, J., Kjeldsen, K. K., … Muresan, I. S. (2014). Sustained mass loss of the northeast Greenland ice sheet triggered by regional warming. *Nature Climate Change*, *4*(4), 292–299. https://doi.org/10.1038/nclimate2161

Kuipers Munneke, P., Smeets, C. J. P. P., Reijmer, C. H., Oerlemans, J., van de Wal, R. S. W., & van den Broeke, M. R. (2018). The K-transect on the western Greenland Ice Sheet: Surface energy balance (2003–2016). *Arctic, Antarctic, and Alpine Research*, *50*(1), e1420952. https://doi.org/10.1080/15230430.2017.1420952

Lachlan-Cope, T., Listowski, C., & O'Shea, S. (2016). The microphysics of clouds over the Antarctic Peninsula – Part 1: Observations. *Atmospheric Chemistry and Physics*, *16*(24), 15605–15617. https://doi.org/10.5194/acp-16-15605-2016

Larsen, N. K., Levy, L. B., Carlson, A. E., Buizert, C., Olsen, J., Strunk, A., … Skov, D. S. (2018). Instability of the Northeast Greenland Ice Stream over the last 45,000 years. *Nature Communications*, *9*(1), 1872. https://doi.org/10.1038/s41467-018-04312-7

Leeson, A. A., Eastoe, E., & Fettweis, X. (2018). Extreme temperature events on Greenland in observations and the MAR regional climate model. *The Cryosphere*, *12*(3), 1091–1102. https://doi.org/10.5194/tc-12-1091-2018

Listowski, C., & Lachlan-Cope, T. (2017). The microphysics of clouds over the Antarctic Peninsula – Part 2: modelling aspects within Polar WRF. *Atmospheric Chemistry and Physics*, *17*(17), 10195–10221. https://doi.org/10.5194/acp-17-10195-2017

Mayer, C., Schaffer, J., Hattermann, T., Floricioiu, D., Krieger, L., Dodd, P. A., … Schannwell, C. (2018). Large ice loss variability at Nioghalvfjerdsfjorden Glacier, Northeast-Greenland. *Nature Communications*, *9*(1), 2768. https://doi.org/10.1038/s41467-018-05180-x

Mernild, S. H., Liston, G. E., van As, D., Hasholt, B., & Yde, J. C. (2018). High-resolution ice sheet surface mass-balance and spatiotemporal runoff simulations: Kangerlussuaq, west Greenland. *Arctic, Antarctic, and Alpine Research*, *50*(1), S100008. https://doi.org/10.1080/15230430.2017.1415856

Mottram, R., Boberg, F., Langen, P. ., Yang, S., Rodehacke, C., Christensen, J. ., & Madsen, M. (2017). Surface mass balance of the Greenland ice sheet in the regional climate model HIRHAM5: Present state and future prospects. *Low Temperature Science*, *75*, 105-115.

Mouginot, J., Rignot, E., Scheuchl, B., Fenty, I., Khazendar, A., Morlighem, M., … Paden, J. (2015). Fast retreat of Zachariæ Isstrøm, northeast Greenland. *Science*, *350*(6266), 1357–1361. https://doi.org/10.1126/SCIENCE.AAC7111

Noël, B., van de Berg, W. J., Machguth, H., Lhermitte, S., Howat, I., Fettweis, X., & van den Broeke, M. R. (2016). A daily, 1 km resolution data set of downscaled Greenland ice sheet surface mass balance (1958–2015). *The Cryosphere*, *10*(5), 2361–2377. https://doi.org/10.5194/tc-10-2361-2016

https://doi.org/10.5194/essd-2019-194
Preprint. Discussion started: 30 October 2019

Polar Weather Research and Forecasting Model, developed by Ohio State University, available from: http://polarmet.osu.edu/PWRF/, last accessed: July 29 2019.

Powers, J. G., Klemp, J. B., Skamarock, W. C., Davis, C. A., Dudhia, J., Gill, D. O., … Duda, M. G. (2017). The Weather Research and Forecasting Model: Overview, System Efforts, and Future Directions. *Bulletin of the American Meteorological Society*, *98*(8), 1717–1737. https://doi.org/10.1175/BAMS-D-15-00308.1

Rignot, E., Fenty, I., Xu, Y., Cai, C., & Kemp, C. (2015). Undercutting of marine-terminating glaciers in West Greenland. *Geophysical Research Letters*, *42*(14), 5909–5917. https://doi.org/10.1002/2015GL064236

Schaffer, J., von Appen, W.-J., Dodd, P. A., Hofstede, C., Mayer, C., de Steur, L., & Kanzow, T. (2017a). Warm water pathways toward Nioghalvfjerdsfjorden Glacier, Northeast Greenland. *Journal of Geophysical Research: Oceans*, *122*(5), 4004–4020. https://doi.org/10.1002/2016JC012462

Sea Surface Temperature and Sea Ice Concentration Data, available from https://rda.ucar.edu/datasets/ds277.7/, last accessed July 29 2019, doi:10.5065/EMOT-ID34

Skamarock, W. C., & Klemp, J. B. (2008). A time-split nonhydrostatic atmospheric model for weather research and forecasting applications. *Journal of Computational Physics*, *227*(7), 3465–3485. https://doi.org/10.1016/j.jcp.2007.01.037

Tedesco, M., Fettweis, X., Mote, T., Wahr, J., Alexander, P., Box, J. E., & Wouters, B. (2013). Evidence and analysis of 2012 Greenland records from spaceborne observations, a regional climate model and reanalysis data. *The Cryosphere*, *7*(2), 615–630. https://doi.org/10.5194/tc-7-615-2013

Turton, J. V., Mölg, T. & Van As, D. (2019a). Atmospheric Processes and Climatological Characteristics of the 79N Glacier (Northeast Greenland). *Monthly Weather Review*, *147*(4), 1375–1394. https://doi.org/10.1175/MWR-D-18-0366.1

Turton, J. V., Mölg, T & Collier, E. (2019b) NEGIS_WRF model output, Open Science Framework Repository, last accessed October 1 2019, doi: /10.17605/OSF.IO/53E6Z.

van As, D., & Fausto, R. (2011). Programme for Monitoring of the Greenland Ice Sheet (PROMICE): first temperature and ablation records. *Geological Survey of Denmark and Greenland Bulletin*, *23*, 73–76.

van den Broeke, M., Box, J., Fettweis, X., Hanna, E., Noël, B., Tedesco, M., … van Kampenhout, L. (2017). Greenland Ice Sheet Surface Mass Loss: Recent Developments in Observation and Modeling. *Current Climate Change Reports*, *3*(4), 345–356. https://doi.org/10.1007/s40641-017-0084-8

Weather Research and Forecasting Model, developed by the National Centre for Atmospheric Research (NCAR). Available from: https://www.mmm.ucar.edu/weather-research-and-forecasting-model, last accessed: October 1 2019.

Wilson, A. B., Bromwich, D. H., & Hines, K. M. (2011). Evaluation of Polar WRF forecasts on the Arctic System Reanalysis domain: Surface and upper air analysis. *Journal of Geophysical Research*, *116*(D11), D11112. https://doi.org/10.1029/2010JD015013